

RSC Advances



This is an *Accepted Manuscript*, which has been through the Royal Society of Chemistry peer review process and has been accepted for publication.

Accepted Manuscripts are published online shortly after acceptance, before technical editing, formatting and proof reading. Using this free service, authors can make their results available to the community, in citable form, before we publish the edited article. This *Accepted Manuscript* will be replaced by the edited, formatted and paginated article as soon as this is available.

You can find more information about *Accepted Manuscripts* in the [Information for Authors](#).

Please note that technical editing may introduce minor changes to the text and/or graphics, which may alter content. The journal's standard [Terms & Conditions](#) and the [Ethical guidelines](#) still apply. In no event shall the Royal Society of Chemistry be held responsible for any errors or omissions in this *Accepted Manuscript* or any consequences arising from the use of any information it contains.



Journal Name

ARTICLE

Beneficial effects of biomimetic nano-sized hydroxyapatite/antibiotic gentamicin enriched chitosan-glycerophosphate hydrogel on the performance of injectable polymethylmethacrylate

Received 00th January 20xx,
Accepted 00th January 20xx

DOI: 10.1039/x0xx00000x

www.rsc.org/

Yue Sa^{ab}, Man Wang^a, Hongbing Deng^c, Yining Wang^{ab}, Tao Jiang^{*ab}

Injectable polymethylmethacrylate (PMMA) bone cement is a widely used bone substitute in cemented arthroplasty, vertebroplasty and osteoporosis fractures. However, due to the inappropriate stiffness, poor bioactivity and high polymerization temperature of PMMA, aseptic loosening of the implanted cement at the bone-cement interface still could be observed in a high rate of patients. To improve the performance of PMMA, artificial extracellular matrices-like chitosan-glycerophosphate (CS-GP) thermos-sensitive hydrogel was introduced into PMMA acting as pore forming agent and osteoconductive nano-sized hydroxyapatite (Nano-HA) /antibiotic gentamicin (GM) carrier. It is shown that CS-GP thermo-sensitive hydrogel can effectively create open pores at the surface of PMMA cement, which is believed to facilitate bone tissue ingrowth and improve the cement anchorage at the bone-cement interface in the future clinical applications. Meanwhile, such hydrogel effectively decreases the maximum polymerization temperature to below 30 °C, prolongs the working time to more than 720 s and produces cement with proper modulus of elasticity and the compressive yield strength range from 402 to 584 MPa and from 3.1 to 5.9 MPa, respectively. Furthermore, the incorporated Nano-HA particles sufficiently increase the mineralization capacity of the cement without compromising its mechanical properties and the incorporated GM remarkably enhance the anti-bacterial activity of the cement. More importantly, Nano-HA and GM enriched CS-GP thermo-sensitive hydrogel effectively improve the overall performance of PMMA cement without influencing the cell survival, suggesting the injectable p-PMMA/CS-GP/Nano-HA/GM cement will hold strong promise for future bone reconstruction applications.

1. Introduction

Bone is the unique tissue in the body that has the strong hardness and forms the skeleton to support the whole body. Despite the fact that bone has the ability of self-regenerating, it often can suffer from major biological and mechanical damages, such as tumour, trauma or congenital disorders, which severely influence the aesthetics, function and psychological well-being of patients.¹ According to a recent survey, the worldwide incidence of bone disorders and conditions has risen sharply over the last decades and is expected to double by 2020.³ Therefore, the effective bone

grafting is necessary and important for the modern quality-of-life expectations. In consideration of the serious disadvantages of donor limit, graft rejection, pathogen transfer, and reimplant injury in conventional therapies, tissue engineering strategy currently opens a new avenue for bone grafting, which utilizes certain biomaterial as a three-dimensional bone substitute for the purpose of bone repair and reconstruction.⁴ In the context of available materials for tissue engineering, the injectable bone substitutes (IBSs) have become increasingly attractive in bone grafting as they offer apparent advantages in view of minimally invasive surgical procedures and effective filling of complex- and irregular- shaped defects with direct contact between biomaterial and surrounding tissue.⁵⁻⁷ From the clinical perspective, the application of IBSs could alleviate patients' discomfort, shorten the recovery time and reduce the treatment cost.⁸

Polymethylmethacrylate (PMMA) or known as "bone cement" is a specialized form of IBS to fix the prosthetic devices for more than 50 years. Until now, PMMA is still a widely used IBS in cemented arthroplasty, vertebroplasty and osteoporosis fractures.⁹⁻¹¹ Although such material has been extensively applied due to its easy handling characteristics, good moldability, sufficient strength, low price and FDA-approved,^{12, 13} it is associated with several unfavourable properties. Aseptic loosening of the implanted PMMA

^a The State Key Laboratory Breeding Base of Basic Science of Stomatology (Hubei-MOST) & Key Laboratory of Oral Biomedicine Ministry of Education, School & Hospital of Stomatology, Wuhan University, 237 Luoyu Road, Wuhan 430079, PR China

^b Department of Prosthodontics, Hospital of Stomatology, Wuhan University, 237 Luoyu Road, Wuhan 430079, PR China

^c Department of Environmental Science, College of Resource and Environmental Science, Wuhan University, 129 Luoyu Road, Wuhan 430079, PR China

* Corresponding author at: The State Key Laboratory Breeding Base of Basic Science of Stomatology (Hubei-MOST) & Key Laboratory of Oral Biomedicine Ministry of Education, School & Hospital of Stomatology, Wuhan University, 237 Luoyu Road, Wuhan 430079, PR China. Tel: +86 27 87686318; Fax: +86 27 87873260. Email address: jiangtao2006@whu.edu.cn

at the cement-bone interface was observed in a high rate of patients due to its inappropriate stiff properties and the poor bioactivity. Thermal necrosis caused by PMMA polymerization resulted in the tissues damage around cement surface. Moreover, the infection of the PMMA caused a number of prosthesis removal in the clinic.¹⁴⁻¹⁶ These behaviours significantly restrict the new bone growth at the bone-cement interface. To circumvent these problems, modifications of PMMA have been performing to improve the PMMA based cement-bone interactions.^{10, 12, 15, 17}

Previous studies confirmed that creating the open porosity was an effective strategy to improve the performance of implanted solid material since the interconnected porous scaffold was believed to relieve the stiffness of material and promote the tissue ingrowth, thereby creating more interlocking and the mechanical anchorage at the bone-material interface.^{4, 12, 18, 19} Van muller and de Wijn *et al* developed the porous PMMA (p-PMMA) by mixing the separated hydrophobic PMMA phase with hydrophilic carboxymethylcellulose (CMC) hydrogel phase.^{18, 20, 21} They found the CMC hydrogel was responsible for creating the porosity and the bone indeed grew into the p-PMMA scaffold.^{20, 21} To modify this system enabling to further improve the performance of p-PMMA, our research group tried to incorporate osteoconductive CaP materials into the CMC hydrogel *in vitro* and *in vivo*.^{10, 15, 22} The *in vitro* study showed that the CMC hydrogel contributed to relieving the stiffness and reducing the risk of thermal necrosis of PMMA material. More importantly, the incorporated CaP provided PMMA cement with potential osteoconductivity without compromising beneficial mechanical properties and the low polymerization temperature of p-PMMA.^{10, 15} However, the following *in vivo* study revealed that the addition of CaP particles did not increase the amount of bone formation and ingrowth at the bone-cement interface.²² The micro-sized β -TCP particles which were embedded in CMC gel previously was found to trigger the host inflammatory response and influence the chemical bonding to bone *in vivo*.²² That suggested the way by which the CaP particles were included into the PMMA matrix previously restricted the osteoconductive advantage of cement. Therefore, new combination of CaP particle and pore forming agent should be further selected and tested to optimize the osteocompatibility of p-PMMA/CaP cement at the interface. In addition to this, since the bone substitute capable of local antibiotic delivery could improve the success rate in revision cases and antibiotic-loaded PMMA cement is becoming the standard practice for preventing infection in joint arthroplasty and for treating infection in osteomyelitis,^{11, 14} antibiotic also need to be considered as an essential component to incorporate into the p-PMMA/CaP system.

To better improve the performance of bone substitute at the bone-material interface, it is preferable to develop biomaterials mimicking the composition and structure of bone in the local sites.²³ Therefore, biomimetic ways to combine artificial extracellular matrices (ECMs)-like hydrogel and nano-sized CaP as a temporary three-dimensional (3-D) environment, which is suitable for suitable cells colonization and eventual tissue regeneration, are currently being broadly explored in the field of chemistry and bone tissue engineering.²⁴⁻²⁶

Chitosan (CS), the unique aminopolysaccharide derived from abundant chitin in the nature, is obtaining great interest for various biomedical applications due to its non-toxic,^{27, 28} biodegradable,^{29, 30}

and anti-bacterial abilities.^{31, 32} Glycerophosphate (GP), an organic compound naturally found in the body, is utilized in treating the unbalance of phosphate metabolism and some type of GP, such as β -GP, has proved acting as an osteogenic supplement when added to cultures of human bone marrow stem cells.³³ Recently, an injectable CS-GP based thermo-sensitive hydrogel was developed and has been becoming more and more attractive in IBS.³³ Such hydrogel could rapidly change their equilibrium swelling via the multiple interactions between CS, β -GP and water under the stimuli of temperature and then form non-free-flowing gel at body temperature (37 °C) from the original solution state.³⁴ In addition, it possesses appealing properties, e.g. injectability, biocompatibility, biodegradability and ability to act as ECM. More importantly, it can serve as a promising carrier for *in situ* release of pre-incorporated osteoconductive CaP particles and pre-loaded drug.^{31, 33, 35} Therefore, CS-GP thermo-sensitive hydrogel could be regarded as an ideal pore forming agent and nano-sized CaP/drug carrier to mimic the mineral component and nanostructure of natural bone at the cement-bone interface. But to the best of our knowledge, no attempt to combine PMMA and CS-GP based thermo-sensitive hydrogel has been reported.

In this study, CS-GP hydrogel was prepared to generate opened and interconnected pores within PMMA. Moreover, osteoconductive nano-sized hydroxyapatite (Nano-HA), which was prepared to mimic the nano-crystals within bone structure,³⁶ or gentamicin (GM), which was used as a broad-spectrum antibiotic for treating infection or osteomyelitis,³⁷ or a combination of them was preloaded into the CS-GP thermo-sensitive hydrogel to modify the bulk properties of the cement. The objective of the present study was to develop a novel injectable PMMA/CS-GP/Nano-HA/GM cement with easy handling property, safe polymerization temperature, adequate biocompatibility, proper mechanical performance, favourable biomineralization capacity and effective infection-resist ability for the future clinical bone reconstruction.

2. EXPERIMENTAL SECTION

2.1 Materials

A two-component (powder and liquid) PMMA kit (Self-curing PMMA, type II) was purchased from Shanghai New Century Dental Materials Co. (Shanghai, China). The solid component consisted of PMMA, dibenzoyl peroxide (BPO), silicon dioxide and barium sulfate powders. The liquid part was a mixture of methylmetacrylate (MMA) solution and N, N-dimethyl-p-toluidine (DMPT) solution. BPO was used as initiator and DMPT was used as accelerator for the polymerization reaction. Silicon dioxide was used as reinforcer and barium sulfate was used as radiopaque agent.

$\text{Ca}(\text{NO}_3)_2 \cdot 4\text{H}_2\text{O}$, $(\text{NH}_4)_2\text{HPO}_4$ and NH_4OH were purchased from Aladdin Co., Ltd. (Shanghai, China). Chitosan (CS) ($M_w = 179.17$ kD; N-deacetylation rate of $\geq 95\%$; viscosity = 100-200 mPa.s) was purchased from Aladdin Co., Ltd. (Shanghai, China). β -GP ($M_w = 216.04$ g/mol) was obtained from Sigma-Aldrich (Sigma-Aldrich, USA). GM sulfate ($M_w = 547.6207$ g/mol, potency ≥ 590 $\mu\text{g}/\text{mg}$) was purchased from Amresco (Amresco, USA). All other chemical reagents were of analytical grade or better.

Table 1. Compositions of the prepared cements.

	Plain PMMA	p-PMMA/CS-GP	p-PMMA/CS-GP/Nano-HA	p-PMMA/CS-GP /GM	p-PMMA/CS-GP /Nano-HA/GM
Solid component (g)					
PMMA	3	3	3	3	3
CS	0	0.09	0.09	0.09	0.09
β -GP	0	0.5	0.5	0.5	0.5
HA	0	0	0.3	0	0.3
GM	0	0	0	0.025	0.025
Liquid component (ml)					
MMA	1.5	1.5	1.5	1.5	1.5
DW	0	0.5	0.5	0.5	0.5

2.2 Preparation and characterization of Nano-HA crystals

Nano-HA was synthesized as our previously described.³⁸ 20 ml of 1.08 M $\text{Ca}(\text{NO}_3)_2 \cdot 4\text{H}_2\text{O}$ (pH=10, adjusted by NH_4OH) was heated to 90 °C and 20 ml of 0.65 M $(\text{NH}_4)_2\text{HPO}_4$ solution was subsequently added drop-wise under stirring. The precipitate was maintained in contact with the reaction solution for 5 h at 90 °C under stirring, and then centrifuged at 1800 *g* for 10 min. After that, the precipitate was repeatedly washed with distilled water (DW) and centrifuged for 6 times, then dried at 37 °C overnight.

The morphological investigation of the synthesized HA precipitate was performed by scanning electron microscope (SEM) (Sigma, Zeiss, Germany) and transmission electron microscope (TEM) (JEM-2100, JOEL, Japan). The crystal phase of synthesized precipitate was analyzed by X-ray diffraction (XRD, X' Pert Pro, The Netherlands) with a wavelength of 1.5406 Å at a voltage of 40 kV and a current of 40 mA. XRD patterns were collected for 2 θ values between 10° and 80° in a continuous mode at a rate of 25 seconds per step and a step size of 0.026° (2 θ).

2.3 Preparation of the cements

In this study, CS-GP thermo-sensitive hydrogel was firstly prepared according to the method of Zhao *et al.*³⁹ In brief, 0.9 g CS powder was dissolved into 4.5 ml 0.1 M hydrochloric acid solution with stirring under room temperature until the complete dissolution of the powder, then the CS solution was chilled at 4 °C for 15 min. Similarly, 0.5 g β -GP liquid was dissolved in DW to a concentration of 50% (w/w) under room temperature and then chilled at 4 °C along with the chitosan solution. Subsequently, β -GP solution was added into CS solution drop-wise under stirring and the CS-GP solution was mixed for another 20 minutes. Then gel-forming process of the solution was conducted in the thermostat at 37 °C for 5 min. To prepare the Nano-HA or GM-loaded thermo-sensitive hydrogel, 300 mg Nano-HA or 25 mg GM or a combination thereof was added into the homogeneous CS-GP solution, respectively. The whole solution was mixed uniformly by using sonication and then transformed into the hydrogel at 37 °C for 5 min (Fig.1).

Table.1 listed the needed raw materials for the cement. To prepare plain PMMA cement, PMMA kit powder part and PMMA kit liquid part were manually blended with the weight ratio of 1:1 (powder weight to liquid weight) until a homogeneous paste was obtained.

Subsequently, the mixture was injected into the Teflon mould (6 mm in diameter; 12 mm in height) to form the cylinder-shaped samples. To prepare the p-PMMA cement, the mixed PMMA phase was further blended with CS-GP hydrogel with a volume ratio of 3:4 until a homogeneous paste was obtained. To prepare the Nano-HA or GM incorporated cements, Nano-HA or GM pre-loaded CS-GP hydrogel was mixed with PMMA paste until a homogeneous mixture was reached. The rest of the process was the same with that of plain PMMA preparation. The schematic diagram of the synthesis of p-PMMA-based cements was shown in Fig. 2. After curing overnight, samples were un moulded, DW washed, freeze-dried and imaged by a Nikon D3100 digital camera.

2.4 Thermal properties and working time

The polymerization temperature of cement was monitored at room temperature of 23.6 °C by a type K thermocouple (Victory high electronic technology co., China) connected to a data logger (Victor E86, Victory high electronic technology co., China). Once the homogeneous mixture was packed into the mould, the probe of the thermocouple was located at the centre of the cement surface according to the previous study.¹⁵ The maximum temperature (T_{max}) was obtained during the polymerization reaction ($n=3$). Further, the working time was recorded, which was defined as the time between the material could be safely injected into a cavity to the material becomes too stiff to inject through the access needle.⁴⁰

2.5 μ -CT analysis

Micro-computed tomography (μ -CT 50, Scanco Medical, Basersdorf, Switzerland) was used to examine the porometrical properties and particle distribution of Nano-HA within the PMMA matrix. A representative cement from each group was placed in a custom-made holder to ensure that the long axis of the cement was oriented perpendicular to the axis of X-ray beam. A pixel of 12 μm , with acquiring conditions of 90 kV and 88 μA in high resolution mode were used. About 900 slices per cement were used to reconstruct the images.

2.6 Porosimetry

The porosity and pore size distribution of cements were evaluated by mercury intrusion porosimeter (MIP; AutoPore IV 9500,

Micrometrics, USA). Three freeze-dried cements from each group were introduced into the penetrometer placed in the low pressure chamber of the porosimeter and filled with mercury for evaluation. The MIP test was performed at a pressure range from 0.0010 to 228.0000 MPa. The relation between pressure p (MPa) and the pore diameter d (μm) was determined by the classic Washburn equation⁴¹ on the basis of a model for cylindrical pores:

$$p = -\frac{4\gamma\cos\theta}{d}$$

where γ is the surface tension of the mercury and θ is the contact angle between the mercury and the pore surface of PMMA. In this study, the Hg surface tension, contact angle of mercury and Hg Density were 485.000 dynes/cm, 130° and 13.5335g/mL, respectively.

2.7 Anti-bacterial activity assay

GM sulfate within the prepared cement was confirmed by detecting S 2p of X-ray photoelectron spectroscopy (XPS; Kratos XSAM 800, Britain) with an Al K α X-ray source (1486.6 eV). The cements were mounted on cement stubs with conductive carbon tape. The take-off angle was fixed at 90° and the pressure in the analysis chamber was 2×10^{-7} Pa. The selected resolution for the general spectra was 100.0 eV of Pass Energy and 1.0 eV/step. The spectra of S 2p were then collected at Pass Energy of 20.0 eV and a step size of 0.05 eV. Finally, XPS results were analysed by XPSPEAK41 software after the subtraction of a linear baseline.

Disk-diffusion method was used to investigate the inhibitory effect of the CS-GP based hydrogel against *Escherichia coli*. 30 μl of the *Escherichia coli* suspensions over the range of 0.05-2 mg/ml were pipetted onto petri dishes containing Luria-Bertani agar culture medium and then distributed evenly. CS-GP hydrogel, CS-GP/Nano-HA hydrogel, CS-GP/GM hydrogel and CS-GP/Nano-HA/GM hydrogel were freeze-dried and pressed into discs (Diameter = 13mm). Then these discs were separately placed onto the semi-solid culture medium for 16 hours incubation at 37°C. After that, the anti-bacterial activities of the prepared composites were evaluated by measuring the zone of inhibition (ZOI), which was defined as the clear region around the disc saturated with an antimicrobial agent on the agar surface. Each sample was repeated three times.

2.8 In vitro cytotoxicity measurement

3-(4, 5-dimethylthiazol-2-yl)-2, 5-diphenyltetrazolium bromide (MTT) assay was carried out to determine the *in vitro* short-term cytotoxicity of the prepared cements. Firstly, MC3T3 cells were routinely cultured in the medium of α -MEM (Hyclone, USA) which was supplemented with 10% fetal bovine serum (FBS; Hyclone,

USA), 1% penicillin (100U/ml) and 1% streptomycin sulphate (100 mg/ml). Then, 200 μl MC3T3 cells were seeded into 96-well microplates at a density of 1×10^4 /well and incubated in a humidified incubator containing 5% CO₂ at 37 °C. After 24 h incubation and attachment, the culture medium was aspirated and replaced with extract solutions ($n=6$). Extracts solutions were prepared by incubating the autoclaving PMMA-based cements in culture medium for 72 h at 37 °C and the ratio between the mass of cements and the final volume of extracts was approximately 0.2 g/ml according to ISO 10993 standard⁴². Standard culture medium alone was served as the negative control. After designed time points (1 d, 3 d), 20 μl MTT (Sigma, USA) solution (5mg/ml) was added to each well, followed by further incubation for 4 h. Subsequently, MTT medium was removed by aspiration and the formed formazan crystals were solubilized by 200 μl dimethyl sulphoxide (DMSO; Amresco, USA) with gently shaking in the dark for 15 min. Lastly, the absorbance was measured using an automated plate reader (Powerwave XS2, Biotek, USA) at a wavelength of 490 nm. The relative growth rate (RGR) was calculated based on the following equation corresponding to cytotoxicity level: $\text{RGR} = \text{OD}_{\text{samples}} / \text{OD}_{\text{negative control}} \times 100\%$.⁴²

2.10 Simulated body fluid (SBF) immersion

In order to assess the reaction of different PMMA cements in physiological conditions, SBF was prepared according to the protocol of Kokubo *et al.*⁴³ The comparison of ion concentrations between SBF and human blood plasma was shown in **Table 2**. The *in vitro* immersion test was carried out by immersing cement in SBF (10 ml SBF for each cement) at 37°C, which was refreshed weekly. After 28 days, cements were washed in DW, freeze-dried, and used for the following studies along with the control cements which was not immersed in SBF.

2.11 Mineralizing capacity of cements

SEM (Sigma, Zeiss, Germany) was used to analyse the internal structure of the freeze-dried cements before and after immersion in SBF. The cross sections of fractured cements were mounted on aluminum stubs using conductive carbon tape and sputter coated with gold. Then the morphology of cements was examined at an accelerating voltage of 5 kV and working distance of 4-8 mm. X-ray Diffraction (XRD; X' Pert Pro, The Netherlands) analysis were used to monitor the composition present in the PMMA cements before and after immersion in SBF. The analysis was performed upon the flat surfaces of cements and the parameters were the same with those of Nano-HA characterization.

Table 2. Ion concentrations, in nM, of SBF and human blood plasma

	Na ⁺	K ⁺	Ca ²⁺	Mg ²⁺	Cl ⁻	SO ₄ ²⁻	HCO ₃ ⁻	HPO ₄ ²⁻
SBF	142.00	5.00	5.00	1.50	152.80	0.50	4.17	2.00
Human blood plasma	142.00	5.00	2.50	1.50	103.00	0.50	27.00	1.00

2.12 Mechanical properties

The modulus of elasticity (E) and the compressive yield strength (σ_y) of cements were determined using a tensile bench (MTS810, MTS Systems co., USA). According to the International Standardization Organization (ISO) ISO 5833, 6 mm×12 mm cylindrical cements ($n=3$) were compressed along their long axis at a cross-head speed of 0.5 mm/min. Unlike the other tests, the mechanical properties were performed immediately after soaking in SBF without intermediate drying of the cements.

2.13 Statistical analysis

A one-way analysis of variance (ANOVA) was used to determine the statistical significance followed by *post hoc* analysis using the Turkey test (SPSS 16.0). Results were considered significantly different at $p < 0.05$.

3. RESULTS AND DISCUSSION

3.1 Confirmation of prepared Nano-HA

Fig. 3a from XRD identifies the crystalline deposit by main reflection peaks for HA (25.8, 31.8, 32.2, 32.9 and 34.0 2θ). Fig. 3b-c reveal needle-shaped HA with average diameter and length of 30 ± 5 nm and 100 ± 20 nm from complementing SEM and TEM observations. Since bone mainly consists of calcium phosphate nanocrystals (~ 70 wt%), the prepared Nano-HA mimics the mineral component of bone with potential osteoconductive capacity.^{8, 24}

3.2 Thermal properties and working time

In this study, we successfully transformed the CS-GP liquid into semisolid hydrogel at physiological conditions ($\text{pH} = 7$, Temperature = 37°C) and synthesized p-PMMA based cements *in vitro* by easily mixing the separated hydrophobic PMMA phase and hydrophilic CS-GP phase. The T_{max} of plain PMMA cement is found to reach up to nearly 80°C (Table 3), which is consistent with the results of previous studies.⁴⁴⁻⁴⁶ However, it is interesting to note that all the p-PMMA based groups show no obvious exothermic reaction with T_{max} varied from 26.7 to 28.3°C (Table 3). No significant difference is found among different p-PMMA based groups ($p > 0.05$). Such result may be attributed to the lower volume density of MMA monomers and higher CS-GP hydrogel in p-PMMA based cements in comparison with those in plain PMMA cement. Therefore, all the p-PMMA based cements mitigate the risk for thermal necrosis to the surrounding tissues. More importantly, the effects of Nano-HA and GM will not be weakened by the polymerization-induced heat during the cements applications.

Table 3. Mean values of T_{max} and working time of the prepared cements

Group	$T_{\text{max}}(^{\circ}\text{C})$	Working time (S)
PMMA	76.9 ± 0.5	516 ± 1.8
p-PMMA/CS-GP	28.3 ± 0.3	723 ± 0.9
p-PMMA/CS-GP/Nano-HA	27.8 ± 1.2	773 ± 1.5
p-PMMA/CS-GP/GM	28.0 ± 0.8	756 ± 0.2
p-PMMA/CS-GP/Nano-HA/GM	26.7 ± 1.0	739 ± 1.3

Since the amount of released heat is closely associated with the polymerization speed of PMMA, the lower T_{max} of p-PMMA based cements resulted in their longer working time. It is found that the working time of p-PMMA based cements varied from 723 to 773 s with no significant difference among groups ($p > 0.05$), which is significantly longer than that of plain PMMA around 516 s ($p < 0.01$) (Table 3). Such result indicates an important clinical significance that surgeons will have enough time to effectively inject the p-PMMA based cement into the complex- and irregular- shaped bone defects without additional techniques in the conventional plain PMMA treatment, such as pre-cooling the cement or decreasing the operation room temperature, to extend the polymerization process⁴⁷.

3.3 Morphology and pore parameters

The surface morphologies of prepared cements are shown in Fig. 4A. In comparison with plain PMMA, numerous pores are found on the surface of p-PMMA based cements. Further, the incorporated Nano-HA particles in white colour are aggregated within the porosities as expected. Since the osteoconductive HA particles can form a direct chemical bond with bone,¹⁷ HA-loaded cements are expected to show better effects for the future bony conjunction when compared with HA-free cements.

The 3D reconstruction images and cross-sectional view from $\mu\text{-CT}$ are used to indicate the bulk morphology of the cement, internal porous structure of PMMA matrix and the incorporated Nano-HA particles (Fig. 4B-C). For the plain PMMA cements, only few pores can be seen outside and inside of the cements. In contrast, the p-PMMA/CS-GP and p-PMMA/CS-GP/GM cements reveal similar irregular porous structures with interconnected channels. For the p-PMMA/CS-GP/Nano-HA and p-PMMA/CS-GP/Nano-HA/GM cements, Nano-HA particles fill the interconnected pores as agglomerated phases. SEM observations at low magnification ($250\times$) further display the general morphologies of cross-sectional cements (Fig. 4D). For the plain PMMA, globular-like MMA particles connect with each other to form the dense structure of PMMA. In comparison, interconnected but irregular porous structures are seen within the other p-PMMA based cements.

Table 4. Cytotoxicity results of the prepared cements and negative control group by MTT assay: Mean of Optical density, RGR and cytotoxicity level.

Group	1d			3d		
	Optical density	RGR(%)	Cytotoxicity level	Optical density	RGR(%)	Cytotoxicity level
PMMA	0.1805±0.0134	128	0	0.2150±0.0287	103	0
p-PMMA/CS-GP	0.1735±0.0102	123	0	0.2225±0.0190	106	0
p-PMMA/CS-GP/Nano-HA	0.1538±0.0197	109	0	0.2703±0.0534	129	0
p-PMMA/CS-GP/GM	0.1470±0.0314	104	0	0.2973±0.0769	142	0
p-PMMA/CS-GP/Nano-HA/GM	0.1450±0.0294	102	0	0.2633±0.0456	126	0
Negative control	0.1415±0.0092	100	0	0.2092±0.0172	100	0

The detailed porosity results are shown in **Fig. 5a**. The porosity with a pore size larger than 10 μm for the PMMA, p-PMMA/CS-GP, p-PMMA/CS-GP/Nano-HA, p-PMMA/CS-GP/GM and p-PMMA/CS-GP/Nano-HA /GM are 0.2%, 8.2%, 5.3%, 10.6% and 5.6%, respectively. Furthermore, the porosity of cements decreases along with the increased pore size. The pore size distribution curve is shown in **Fig. 5b**. The peaks representing the average pore diameters correspond to pore sizes of 6 μm , 76.5 μm , 88.4 μm , 77.8 μm and 69.9 μm for PMMA, p-PMMA/CS-GP, p-PMMA/CS-GP/Nano-HA, p-PMMA/CS-GP/GM and p-PMMA/CS-GP/ Nano-HA /GM, respectively (**Fig. 5b**). The morphology and MIP results both reveal that only a few separated pores were involved in plain PMMA due to the introduction of air during the plain PMMA preparation. In contrast, open porosities with pore interconnectivity are found in p-PMMA based cements. Although p-PMMA/CS-GP/Nano-HA cement and p-PMMA/CS-GP/Nano-HA/GM cement both show decreased porosities in comparison with p-PMMA/CS-GP cement and p-PMMA/CS-GP/GM cement due to the incorporation of Nano-HA particles, all the p-PMMA based cements prove that CS-GP hydrogel formed a continuous phase after preparation of the cement. It is known that the hydrogel mimics the native ECM both in mechanical and compositional properties.^{33, 48} Therefore, the CS-GP hydrogel can serve as a supporting network in cements for cells during tissue regeneration, which is believed to benefit the future bone ingrowth into the cement *in vivo*.

3.4 Evidence of Anti-bacterial activity

The XPS spectra confirm the successfully incorporated GM sulfate in group p-PMMA/CS-GP/GM and group p-PMMA/CS-GP/Nano-HA/GM by identifying the single type of S 2p at the binding energy about 168.5 eV. However, no obvious S 2p peak is found in group plain PMMA (**Fig. 6A**). The inhibition abilities of the CS-GP based hydrogels are shown in **Fig. 6B**. It is found that all the measured plates show the translucent zone against *Escherichia coli*. Furthermore, group p-PMMA/CS-GP/GM and group p-PMMA/CS-GP/Nano-HA/GM display greater diameters of ZOI (4.58 cm and 4.39 cm, respectively) than those of p-PMMA/CS-GP and p-PMMA/CS-GP/Nano-HA (0.35 cm and 0.29 cm, respectively) (**Fig. 6B**). No statistical significance is found between group p-PMMA/CS-GP and group p-PMMA/CS-GP/Nano-HA ($p > 0.05$) or between p-PMMA/CS-GP/GM and group p-PMMA/CS-GP/Nano-HA/GM ($p > 0.05$). Such result indicates that CS component involved in CS-GP hydrogel indeed plays a certain part in the antibacterial activity. But the addition of GM remarkably enhances the antibacterial activity

of the cement suggesting the better infection control abilities of GM loaded cements in future *in vivo* applications.

3.5 *In vitro* cytotoxicity measurement

To better adapt the *in vivo* circumstance, the cytotoxicity of cement is also of great concern. The results are shown in **Table 4**. It is evident that the OD values increase with the culture time for all the cements. Accordingly, the RGR of MC3T3 cells are higher than 100% in the presence of all cements both in the 1st day and the 3rd day. There is no statistically significant difference among all groups as compared to the control ($p > 0.05$). Such result proves that plain PMMA supports the cell viability, which is consistent with previous studies that PMMA showed no cytotoxicity.¹⁷ More interestingly, the addition of CS-GP, Nano-HA and GM did not influence the cell survival, suggesting the modifications of plain PMMA could remarkably improve the overall performance of cements without disturbing the cell viability.

3.6 Mineralizing capacity of cements

SEM observations in high magnifications (20,000 \times) confirm the mineral formation abilities of the cements (**Fig. 7A**). Before immersion, group PMMA show clear surface of PMMA matrix. Group p-PMMA/CS-GP and group p-PMMA/CS-GP/GM display uniformly formed CS/GP films covering the PMMA matrix. Group p-PMMA/CS-GP/Nano-HA and group p-PMMA/CS-GP/Nano-HA/GM reveal the incorporated needle-like Nano-HA crystals lay on the CS-GP films. After immersion in SBF for 28 days, no obvious change is found in group PMMA and only a few granular precipitates are distributed on the surface of PMMA matrix in group p-PMMA/CS-GP and group p-PMMA/CS-GP/GM. In contrast, abundant and bigger ball-like precipitates form a layer on the surfaces of needle-like Nano-HA crystals as well as the surface of PMMA matrix in group p-PMMA/CS-GP/Nano-HA and group p-PMMA/CS-GP/Nano-HA/GM (**Fig. 7A**).

Fig. 7B presents the detected crystal phases from XRD analysis before and after immersing cements in SBF. Before immersion, a typical peak corresponding to barium sulfate (at 27.0° 2 θ) is detected for all the cements and a typical peak corresponding to HA is identified (at 32.0° 2 θ) for the HA loaded cements. After immersion for 28 days, no obvious change is observed for group PMMA. A peak assigned to the reflection of an apatite-like phase (at 31.9° 2 θ) is identified for all p-PMMA based groups.

Taking inspiration from the mineral component of natural bone, a carbonated apatite nanocrystal, we incorporated Nano-HA into the CS-GP hydrogel to facilitate the mineral-forming ability. SEM observations and XRD identification prove that plain PMMA did not interact with SBF and Nano-HA free p-PMMA cements only showed slight interaction with SBF. These phenomena agree with previous study where plain PMMA was bioinert and CS incorporation induced the formation of a few apatitic precipitates onto the surface of PMMA due to the CS composition and the beneficial surface roughness as well as the wettability of PMMA perfected by CS⁴⁹. In contrast, Nano-HA loaded p-PMMA show agglomerations of Nano-HA particles within the porosities after preparation. Further, a dense ball-like apatite layer forms on the surface of Nano-HA particles after immersion in SBF for 28 days. It is known that some bioactive IBS, like calcium phosphate cement, show ability of forming apatite-like structure in the SBF.¹⁰ Evidently, SEM and XRD results prove that effectively incorporated osteoconductive Nano-HA particles provide better mineral forming ability of cements, which evidently improve the potential bioactivity of injectable p-PMMA/CS-GP/Nano-HA/GM cement for future *in vivo* bone-bonding in comparison with injectable bioinert PMMA.

3.7 Mechanical properties

Mechanical results are displayed in Fig. 8. Before immersion, plain PMMA cement show E of 5107.31 MPa and σ_y of 62.31 MPa. p-PMMA based cements reveal the E values range from 402 to 584 MPa and σ_y values range from 3.1 to 5.9 MPa. The E and σ_y values of PMMA cement are significantly higher than those of p-PMMA based cements ($p < 0.001$). No significant difference of E and σ_y is found among p-PMMA based cements ($p > 0.05$). After immersion in SBF for 28 days, no statistical significance is found between the two time points regarding both σ_y and E for all the groups ($p > 0.05$). Mechanical properties play influential roles in determining the long-term stability of biomaterials. Due to this, the stiffness of plain PMMA makes the poor bone-PMMA integration which causes the occurrence of interface fractures.¹⁰ Furthermore, the weak strength of the hydrogel restricts its application only in cartilage reconstructions or small bone defects under the non-load-bearing condition^{8,31}. However, the mechanical results in the present study reveal the interesting compromise between plain PMMA and CS-GP hydrogel. All the p-PMMA based cements well match the strength and stiffness of cancellous bone (50~800 MPa of E and 4~12 MPa of σ_y , respectively),^{50, 51} which are significantly lower than injectable plain PMMA but higher than injectable hydrogels.⁵²⁻⁵⁴ Further, since the mechanical properties of p-PMMA cements are mainly determined by PMMA *per se* and pore forming agent^{10,12,15} and the addition of Nano-HA or GM or a combination thereof within the pore forming agent do not significantly influence the amount of CS-GP hydrogel, all the modified p-PMMA cements show similar bulk mechanical properties which will be highly beneficial in view of possible stress shielding effects and corresponding reduction of the fracture risk when compared with conventional plain PMMA of much higher strength and stiffness.^{55,56}

4. CONCLUSION

The present *in vitro* study demonstrates that the appropriate selection of instructive components is the key strategy to improve the properties of constructed cements. Specifically, CS-GP thermo-sensitive hydrogel creates open pores at the surface of PMMA cement, which is believed to facilitate bone tissue ingrowth and improve the cement anchorage at the bone-cement interface in the future clinical applications. Furthermore, CS-GP hydrogel decreases the T_{max} , prolonged the working time, and make appropriate mechanical properties of cements. Enriched Nano-HA particle within hydrogel enhances the mineralization capacity of the cements without compromising their mechanical properties. Enriched GM within hydrogel improves the anti-bacterial activity of cements, which will benefit the prevention of infections. Ultimately, Nano-HA and GM enriched CS-GP hydrogel increase the overall performance of PMMA cement without influencing the cell survival, suggesting the injectable p-PMMA/CS-GP/Nano-HA/GM cement would hold strong promise for future bone reconstruction applications.

Acknowledgements

This work was supported by the National Natural Science Foundation of China (No. 81470771, No. 81500887), and the Fundamental Research Funds for the Central Universities (No. 2042015kf0093).

Notes and references

1. F. Akhlaghi and F. Aframian-Farnad, *Journal of oral and maxillofacial surgery*, 1997, **55**, 927-930.
2. A. Biswas, I. S. Bayer, H. Zhao, T. Wang, F. Watanabe and A. S. Biris, *Biomacromolecules*, 2010, **11**, 2545-2549.
3. A. R. Amini, C. T. Laurencin and S. P. Nukavarapu, *Critical reviews in biomedical engineering*, 2012, **40**, 363-408.
4. X. Liu, K. Zhao, T. Gong, J. Song, C. Bao, E. Luo, J. Weng and S. Zhou, *Biomacromolecules*, 2014, **15**, 1019-1030.
5. S. Larsson and G. Hannink, *Injury*, 2011, **42 Suppl 2**, S30-34.
6. J. F. Mano, R. A. Sousa, L. F. Boesel, N. M. Neves and R. L. Reis, *Composites Science and Technology*, 2004, **64**, 789-817.
7. M. Bongio, J. J. van den Beucken, S. C. Leeuwenburgh and J. A. Jansen, *Journal of tissue engineering and regenerative medicine*, 2015, **9**, 191-209.
8. M. Bongio, J. J. van den Beucken, M. R. Nejadnik, Z. Tahmasebi Birgani, P. Habibovic, L. A. Kinard, F. K. Kasper, A. G. Mikos, S. C. Leeuwenburgh and J. A. Jansen, *Acta biomaterialia*, 2013, **9**, 5464-5474.
9. W. M. Lam, H. B. Pan, M. K. Fong, W. S. Cheung, K. L. Wong, Z. Y. Li, K. D. Luk, W. K. Chan, C. T. Wong, C. Yang and W. W. Lu, *Journal of biomedical materials research. Part B, Applied biomaterials*, 2011, **96**, 76-83.

10. M. A. Lopez-Heredia, Y. Sa, P. Salmon, J. R. de Wijn, J. G. Wolke and J. A. Jansen, *Acta biomaterialia*, 2012, **8**, 3120-3127.
11. H. Tan, Z. Peng, Q. Li, X. Xu, S. Guo and T. Tang, *Biomaterials*, 2012, **33**, 365-377.
12. M. Shi, J. D. Kretlow, A. Nguyen, S. Young, L. Scott Baggett, M. E. Wong, F. K. Kasper and A. G. Mikos, *Biomaterials*, **31**, 4146-4156.
13. J. D. Kretlow, M. Shi, S. Young, P. P. Spicer, N. Demian, J. A. Jansen, M. E. Wong, F. K. Kasper and A. G. Mikos, *Tissue engineering. Part C, Methods*, 2010, **16**, 1427-1438.
14. K. W. Lye, H. Tideman, M. A. Merckx and J. A. Jansen, *Tissue engineering. Part B, Reviews*, 2009, **15**, 485-496.
15. Y. Sa, F. Yang, S. C. Leeuwenburgh, J. G. Wolke, G. Ye, J. R. de Wijn, J. A. Jansen and Y. Wang, *Journal of biomedical materials research. Part B, Applied biomaterials*, 2015, **103**, 548-555.
16. K. W. Lye, S. Lee, H. Tideman, M. A. Merckx and J. A. Jansen, *International journal of oral and maxillofacial surgery*, 2011, **40**, 86-93.
17. Q. He, H. Chen, L. Huang, J. Dong, D. Guo, M. Mao, L. Kong, Y. Li, Z. Wu and W. Lei, *PLoS one*, 2012, **7**, e42525.
18. J. R. de Wijn, *Catholic University, Nijmegen*, 1982.
19. S. J. Hollister, *Nature materials*, 2005, **4**, 518-524.
20. M. L. Bruens, H. Pieterman, J. R. de Wijn and J. M. Vaandrager, *The Journal of craniofacial surgery*, 2003, **14**, 63-68.
21. P. J. van Mullem, J. R. de Wijn and J. M. Vaandrager, *Annals of plastic surgery*, 1988, **21**, 576-582.
22. K. W. Lye, H. Tideman, J. C. Wolke, M. A. Merckx, F. K. Chin and J. A. Jansen, *Clinical oral implants research*, 2013, **24**, 100-109.
23. H. Shin, S. Jo and A. G. Mikos, *Biomaterials*, 2003, **24**, 4353-4364.
24. M. Bongio, J. Van Den Beucken, M. Nejadnik, S. Leeuwenburgh, L. Kinard, F. Kasper, A. Mikos and J. Jansen, *European cells & materials*, 2011, **22**, 359-376.
25. G. Liu, D. Zhao, A. P. Tomsia, A. M. Minor, X. Song and E. Saiz, *Journal of the American Chemical Society*, 2009, **131**, 9937-9939.
26. S. A. Hutchens, R. S. Benson, B. R. Evans, H. M. O'Neill and C. J. Rawn, *Biomaterials*, 2006, **27**, 4661-4670.
27. J. Wu, W. Wei, L. Y. Wang, Z. G. Su and G. H. Ma, *Biomaterials*, 2007, **28**, 2220-2232.
28. H. Jiang, Y. Zuo, Q. Zou, H. Wang, J. Du, Y. Li and X. Yang, *ACS applied materials & interfaces*, 2013, **5**, 12036-12044.
29. H. Deng, P. Lin, S. Xin, R. Huang, W. Li, Y. Du, X. Zhou and J. Yang, *Carbohydrate polymers*, 2012, **89**, 307-313.
30. G. Wang, L. Zheng, H. Zhao, J. Miao, C. Sun, H. Liu, Z. Huang, X. Yu, J. Wang and X. Tao, *ACS applied materials & interfaces*, 2011, **3**, 1692-1701.
31. Y. Tang, Y. Du, Y. Li, X. Wang and X. Hu, *Journal of biomedical materials research. Part A*, 2009, **91**, 953-963.
32. H. Deng, X. Li, B. Ding, Y. Du, G. Li, J. Yang and X. Hu, *Carbohydrate polymers*, 2011, **83**, 973-978.
33. H. Y. Zhou, L. J. Jiang, P. P. Cao, J. B. Li and X. G. Chen, *Carbohydrate polymers*, 2015, **117**, 524-536.
34. Y. Samchenko, Z. Ulberg and O. Korotych, *Advances in colloid and interface science*, 2011, **168**, 247-262.
35. Q. Peng, X. Sun, T. Gong, C. Y. Wu, T. Zhang, J. Tan and Z. R. Zhang, *Acta biomaterialia*, 2013, **9**, 5063-5069.
36. D. Li, H. Sun, L. Jiang, K. Zhang, W. Liu, Y. Zhu, J. Fangteng, C. Shi, L. Zhao and B. Yang, *ACS applied materials & interfaces*, 2014, **6**, 9402-9410.
37. F. Pishbin, V. Mourino, S. Flor, S. Kreppel, V. Salih, M. P. Ryan and A. R. Boccaccini, *ACS applied materials & interfaces*, 2014, **6**, 8796-8806.
38. T. Jiang, X. Ma, Z. Wang, H. Tong, J. Hu and Y. Wang, *Journal of dentistry*, 2008, **36**, 907-914.
39. Q. S. Zhao, Q. X. Ji, K. Xing, X. Y. Li, C. S. Liu and X. G. Chen, *Carbohydrate Polymers*, 2009, **76**, 410-416.
40. M. Timothy S. Eckel, MD, and Wayne Olan, MD, *Elsevier Inc*, 2009, **12**, 44-50.
41. E. W. Washburn, *Physical review*, 1921, **17**, 273.
42. G. Meric, J. E. Dahl and I. E. Ruyter, *Dental Materials*, 2008, **24**, 1201-1206.
43. T. Kokubo, H. Kushitani, S. Sakka, T. Kitsugi and T. Yamamuro, *Journal of biomedical materials research*, 1990, **24**, 721-734.
44. E. Euler, J. Bauer, L. Jonck and T. Kreusser, *Der Unfallchirurg*, 1989, **92**, 606.
45. K. F. Abdel-Kader, S. Allcock, D. I. Walker and S. B. Chaudhry, *The Journal of arthroplasty*, 2001, **16**, 811-819.
46. S. H. Oh, S. Y. Choi, S. H. Choi, Y. K. Lee and K. N. Kim, *Journal of materials science*, 2004, **15**, 25-33.
47. C. F. Hohmann and J. Berger-Sweeney, *Perspectives on developmental neurobiology*, 1998, **5**, 401-425.
48. K. Y. Lee and D. J. Mooney, *Chemical reviews*, 2001, **101**, 1869-1879.
49. H. Tan, S. Guo, S. Yang, X. Xu and T. Tang, *Acta biomaterialia*, 2012, **8**, 2166-2174.
50. S. Yang, K.-F. Leong, Z. Du and C.-K. Chua, *Tissue engineering*, 2001, **7**, 679-689.
51. G. Baroud, J. Nemes, P. Heini and T. Steffen, *Eur Spine J*, 2003, **12**, 421-426.
52. L. Wang, D. M. Yoon, P. P. Spicer, A. M. Henslee, D. W. Scott, M. E. Wong, F. K. Kasper and A. G. Mikos, *Journal of Biomedical Materials Research Part B: Applied Biomaterials*, 2013, **101**, 813-825.
53. X. Z. Zhang, P. Jo Lewis and C. C. Chu, *Biomaterials*, 2005, **26**, 3299-3309.
54. X. Z. Zhang, D. Q. Wu and C. C. Chu, *Biomaterials*, 2004, **25**, 3793-3805.
55. G. Baroud, C. Vant and R. Wilcox, *Journal of long-term effects of medical implants*, 2006, **16**, 265-280.
56. G. Baroud and M. Bohner, *Joint, bone, spine : revue du rhumatisme*, 2006, **73**, 144-150.

Fig.1. Different status of CS-GP solution at room and body temperature. All groups of CS-GP solution remained liquid at room temperature (23.6°C) and transformed into semisolid hydrogel at body temperature (37°C).

Fig.2. The schematic diagram of the synthesis of p-PMMA-based cements.

Fig.3. Characterizations of Nano-HA particles. (a) XRD analysis, (b) SEM observation, and (c) TEM observation

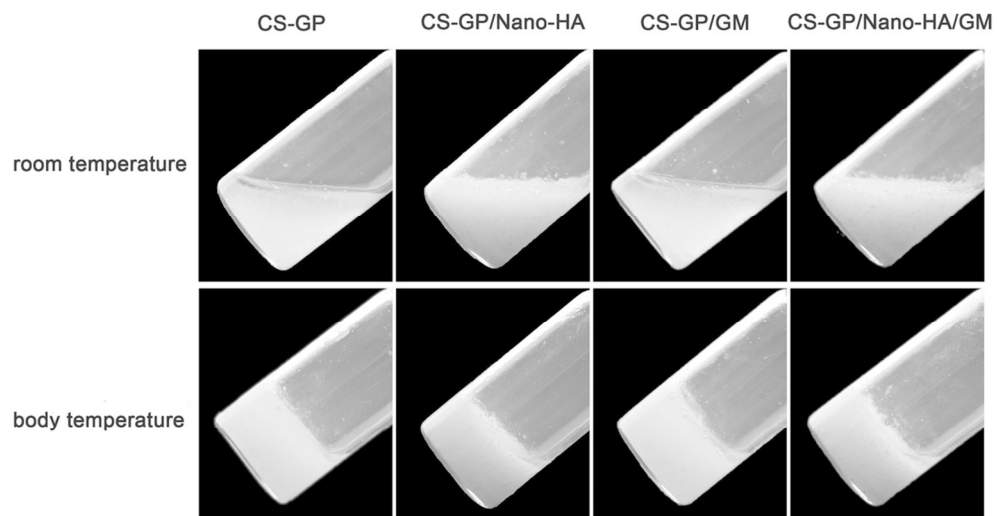
Fig.4. Morphology of the CS-GP hydrogel and prepared cements (A) Surface morphologies; (B,C) μ -CT graphs and (D) SEM observations at low magnification.

Fig.5. Porometric properties of PMMA-based cements: a. porosity; b. pore-size distributions.

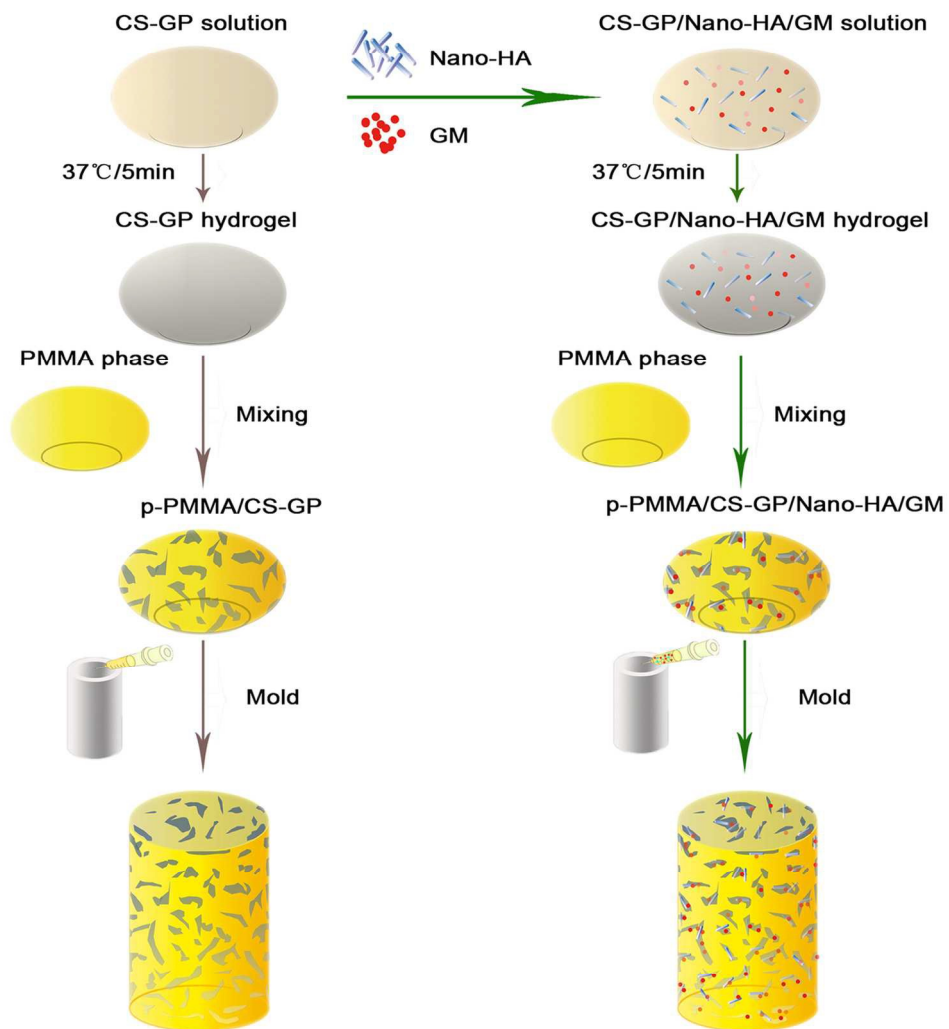
Fig.6. Evidence of antibacterial activity of cements (A) XPS spectra of S 2p for the solid PMMA and GM-loaded PMMA cements; (B) Antibacterial activity of disc-like samples by Zone of inhibition (ZOI) test against E.coli: a. CS-GP; b. CS-GP/Nano-HA; c. CS-GP/GM; d. CS-GP/Nano-HA/GM. (Translucent zones indicated inhibition of bacterial growth).

Fig.7. Mineralizing capacity of cements. (A) SEM images ($\times 20000$) and (B) XRD patterns of PMMA-based cements before and after immersion in SBF for 28 days

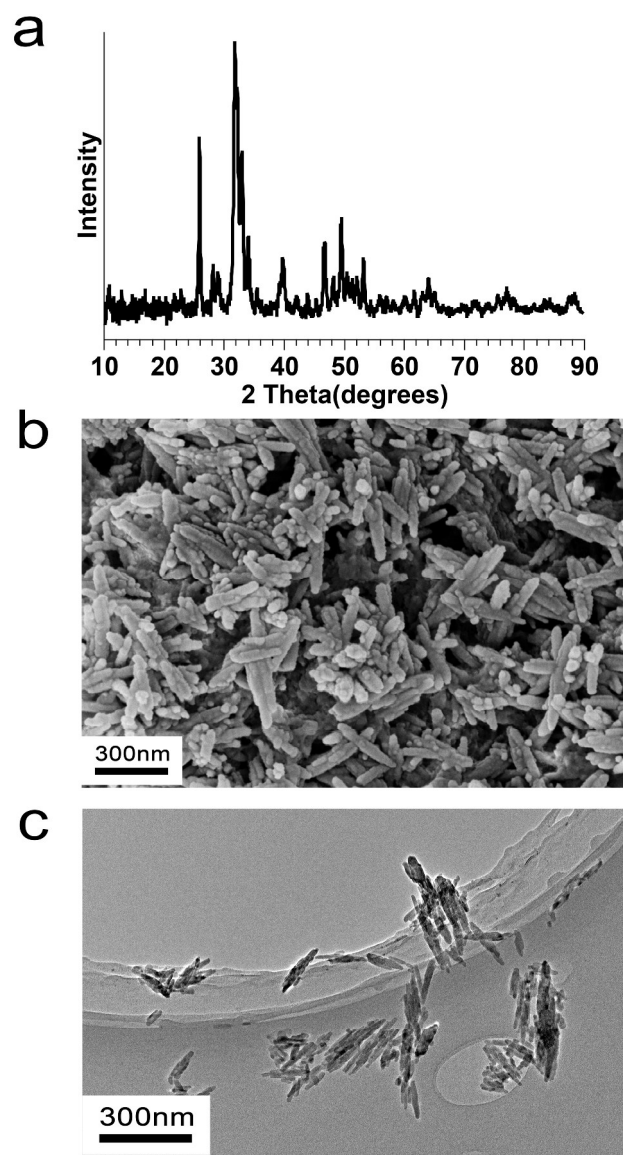
Fig.8. Mechanical properties of PMMA-based cements before and after immersion in SBF for 28 days. (I). PMMA; (II). p-PMMA/CS-GP; (III). p-PMMA/CS-GP/Nano-HA; (IV). p-PMMA/CS-GP/GM; (V). p-PMMA/CS-GP/Nano-HA/GM. a. Modulus of elasticity (E); b. Compressive yield strength (σ_y). (* shows significant difference between plain PMMA and other groups regarding E or σ_y , $P < 0.05$)

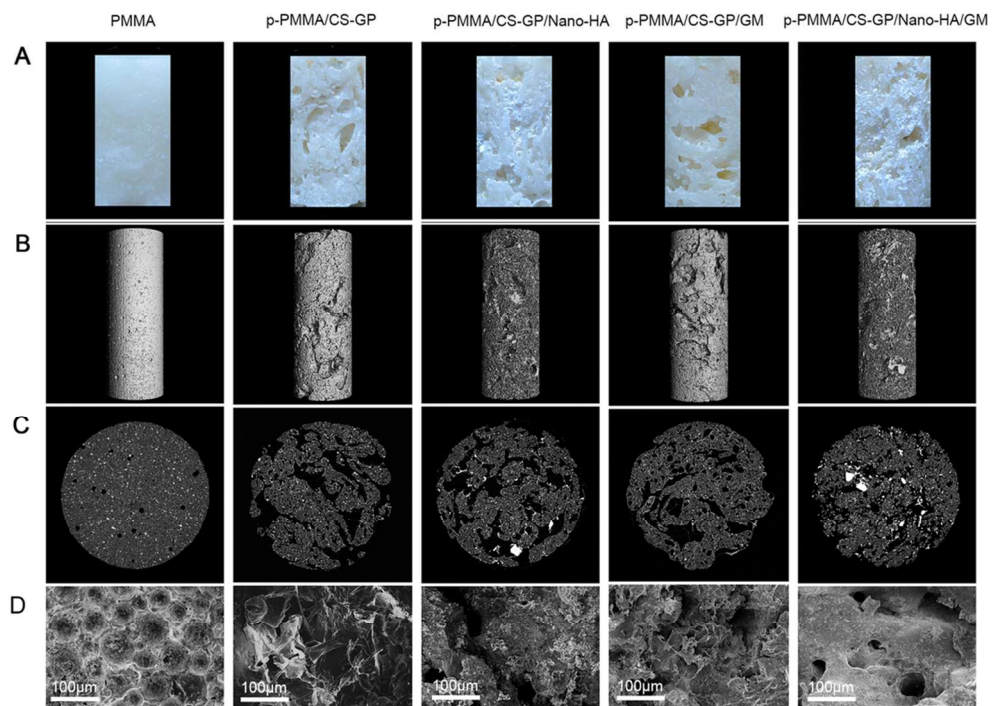


49x26mm (600 x 600 DPI)

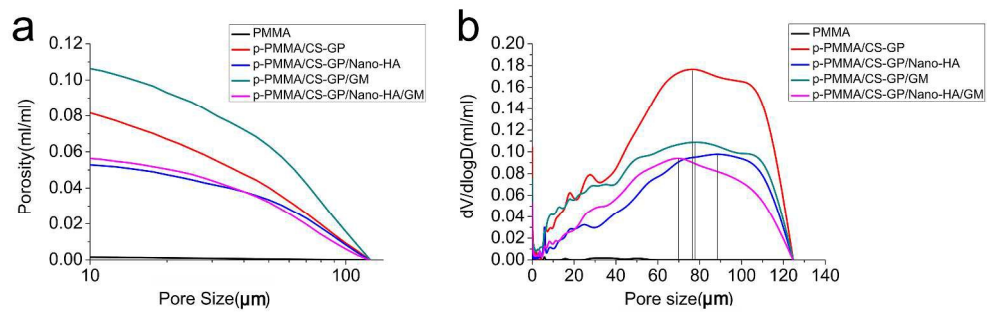


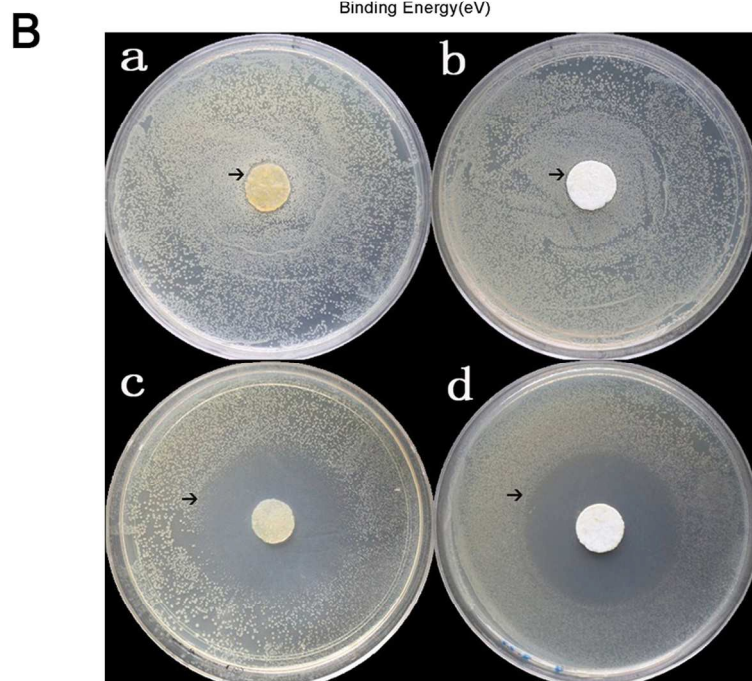
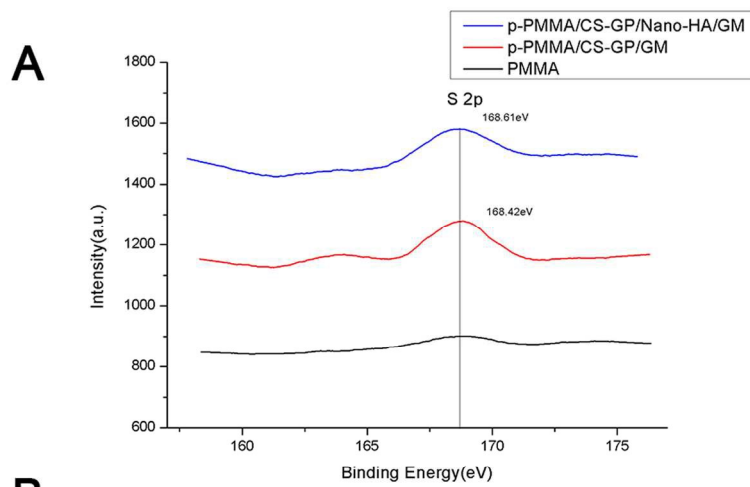
71x80mm (600 x 600 DPI)



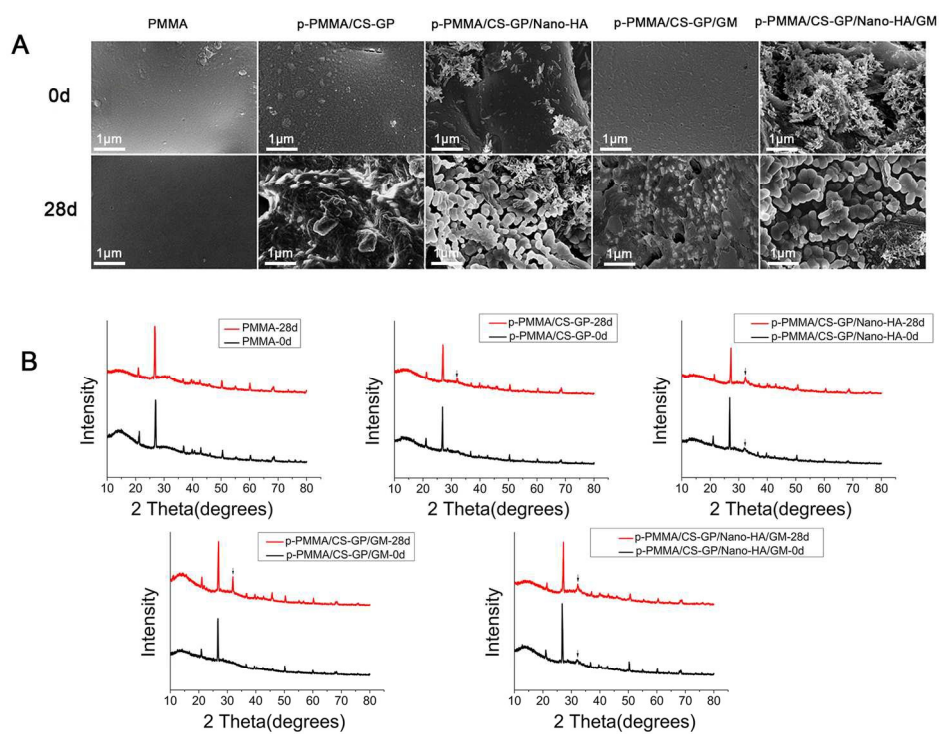


49x36mm (600 x 600 DPI)

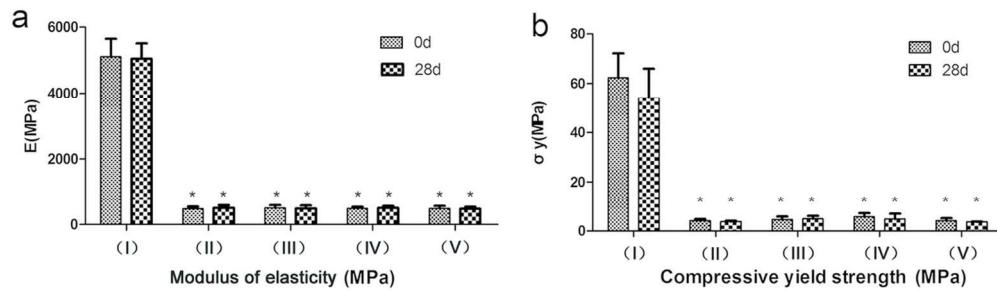




80x111mm (600 x 600 DPI)



99x77mm (600 x 600 DPI)



59x18mm (600 x 600 DPI)